Contents

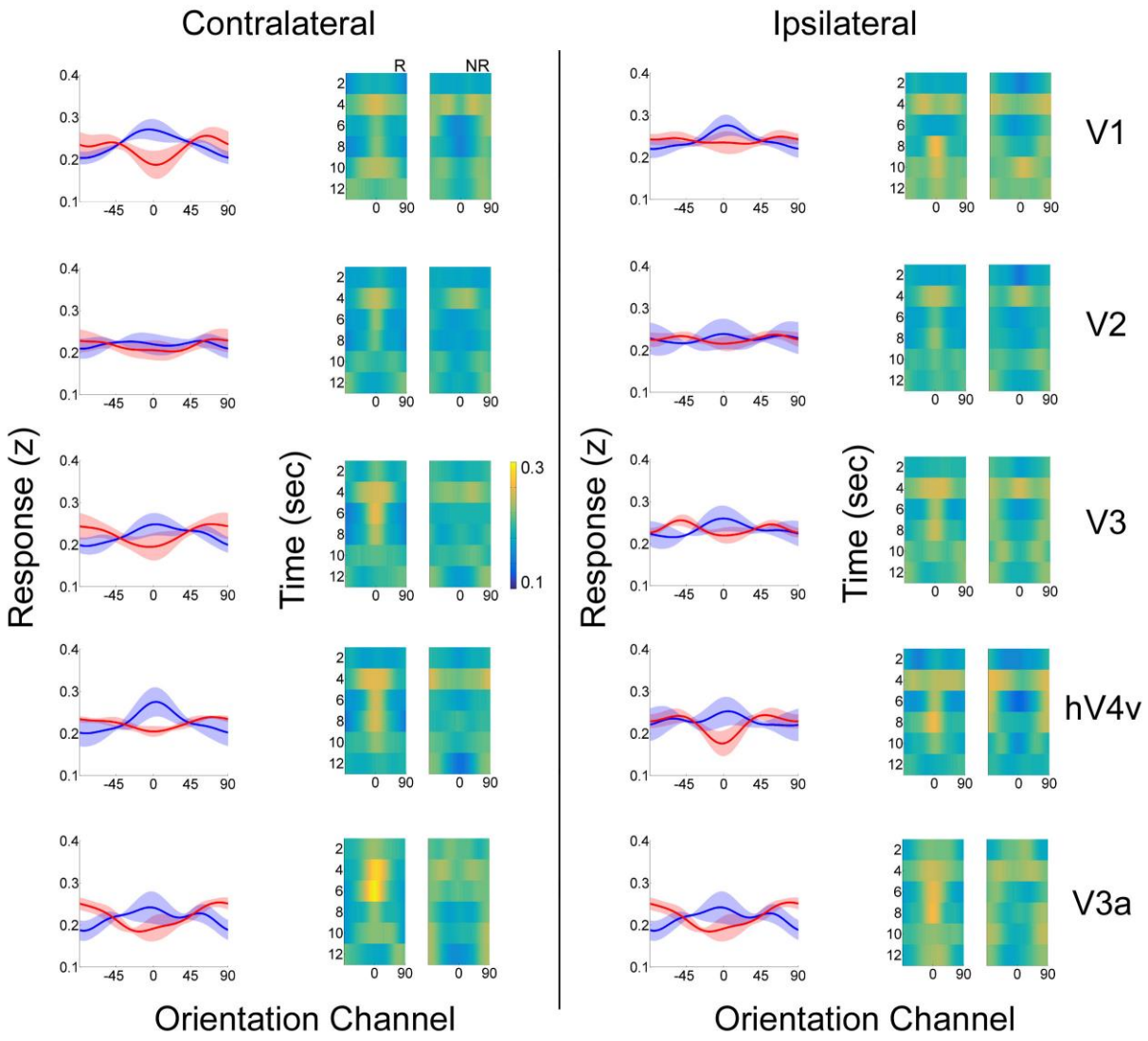

Figure S1. Reconstructions of the remembered and non-remembered orientations in retinotopically organized visual cortex. Related to *Reconstructions of Orientation in Retinotopically Organized Visual and Posterior Parietal Cortex*, Results. The left column of each panel plots reconstructions of the remembered (blue) and non-remembered (red) orientations using activation patterns averaged over a period spanning 8-12 seconds after the onset of the sample display. Each row depicts data from a single visual area (e.g., V1, V2, V3; see labels at far right). Shaded regions are ±1 S.E.M. The right column of each panel plots reconstructions of the remembered ("R") and non-remembered ("NR") orientations measured on a time point-by-time point basis. Time is relative to the onset of the sample display, and all plots have the same color scale. Note that the time-averaged plots shown in the left column were obtained by applying an IEM to activation patterns averaged over samples acquired 8, 10, and 12 seconds after the onset of the sample display. Thus, there is not a direct correspondence between these plots and the sample-by-sample plots in the right column.

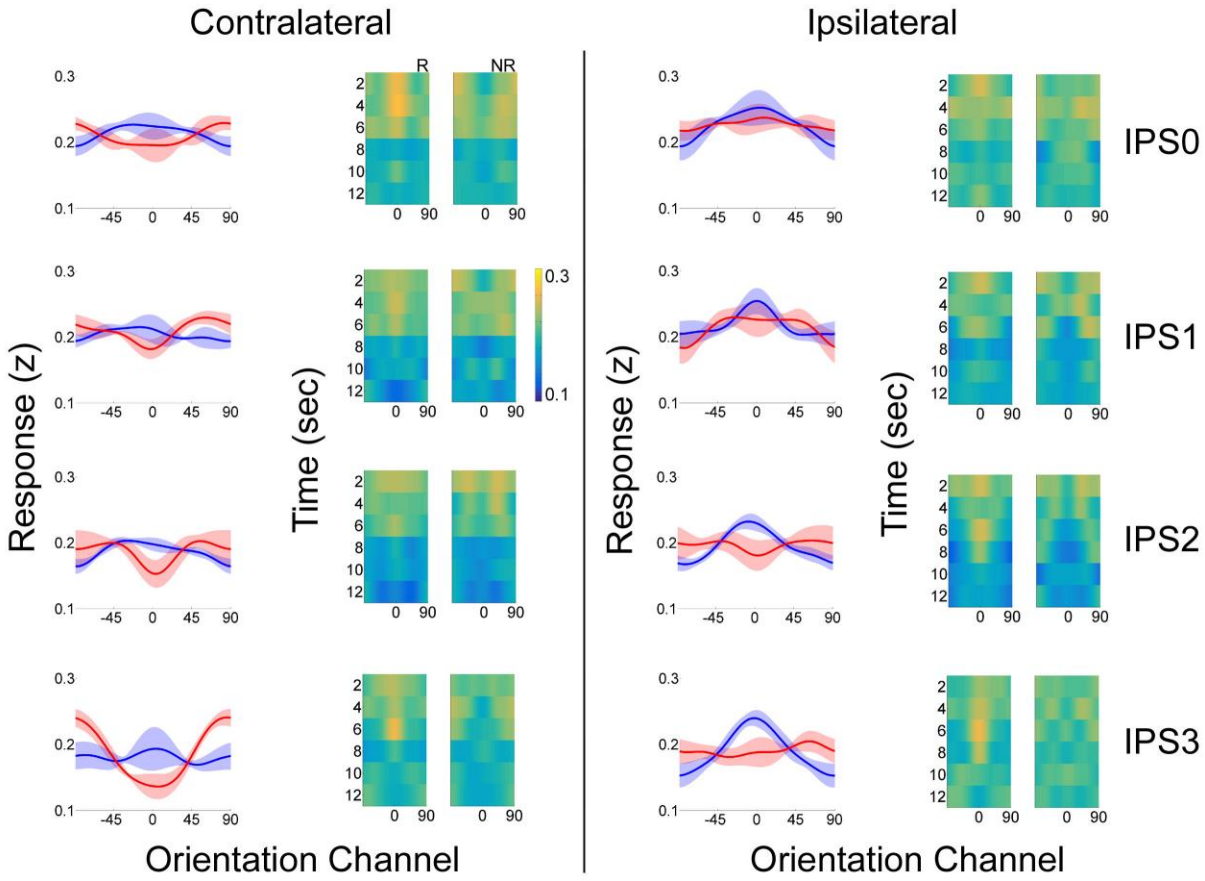

Figure S2. Reconstructions of the remembered and non-remembered orientations in retinotopically organized posterior parietal cortex. Related to *Reconstructions of Orientation in Retinotopically Organized Visual and Posterior Parietal Cortex*, Results. The left column of each panel plots reconstructions of the remembered (blue) and non-remembered (red) orientations using data averaged over a period spanning 8-12 seconds after the onset of the sample display. Each row depicts data from a single IPS subregion (e.g., IPS0, IPS1, etc.; see labels at far right). Shaded regions are ±1 S.E.M. The right column of each panel plots reconstructions of the remembered ("R") and non-remembered (NR) orientations measured on a time point-by-time point basis. Time is relative to the onset of the sample display, and all plots have the same color scale. Note that the time-averaged plots shown in the left column were obtained by applying an IEM to activation patterns averaged over samples acquired 8, 10, and 12 seconds after the onset of the sample display. Thus, there is not a direct correspondence between these plots and the sample-by-sample plots in the right column.

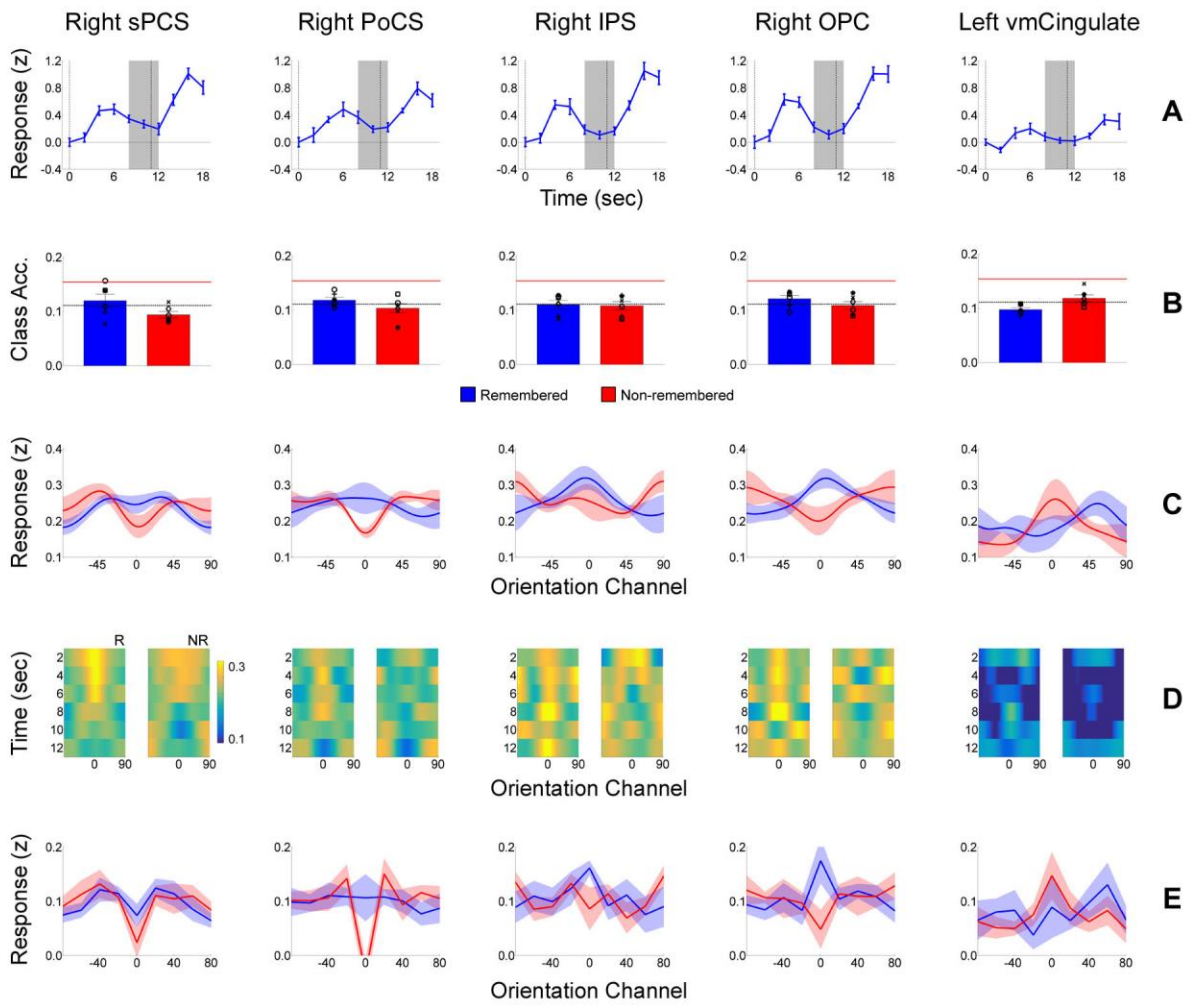

Figure S3 (Part 1). Representations of the remembered and non-remembered orientations in cortical regions with elevated delay period activation. Related to Figure 4. We used a random-effects general linear model containing regressors marking the sample, delay, and probe epochs to identify cortical regions showing elevated delay period activation (see Supplemental Experimental Procedures). Row A: estimated BOLD responses time-locked to the onset of the sample display. The vertical dashed lines at 0 and 11 seconds mark the onsets of the sample and probe displays, respectively. The shaded grey region marks data points used for subsequent multivariate analyses in rows C-F. Error bars are ±1 within-participant S.E.M. Row B: multivariate classification accuracy for the remembered and non-remembered orientations. Black symbols correspond to individual participants. The horizontal dashed line at 0.1111 marks idealized chance-level classification accuracy, while the horizontal red line at approximately 0.15 marks empirical chance-level classifier performance given the number of trials that each participant performed (see Supplemental Experimental Procedures). Row C: reconstructions of

the remembered and non-remembered orientations obtained using an inverted encoding model. Shaded areas are ±1 within-participant S.E.M. Row D: Reconstructions of the remembered ("R") and non-remembered ("NR") orientation on a sample-by-sample basis. All panels are on the same color scale (see color bar). Row E: reconstructions of the remembered and non-remembered orientations obtained using a basis set of Kroeneker delta functions. Shaded areas are ±1 within-participant S.E.M.

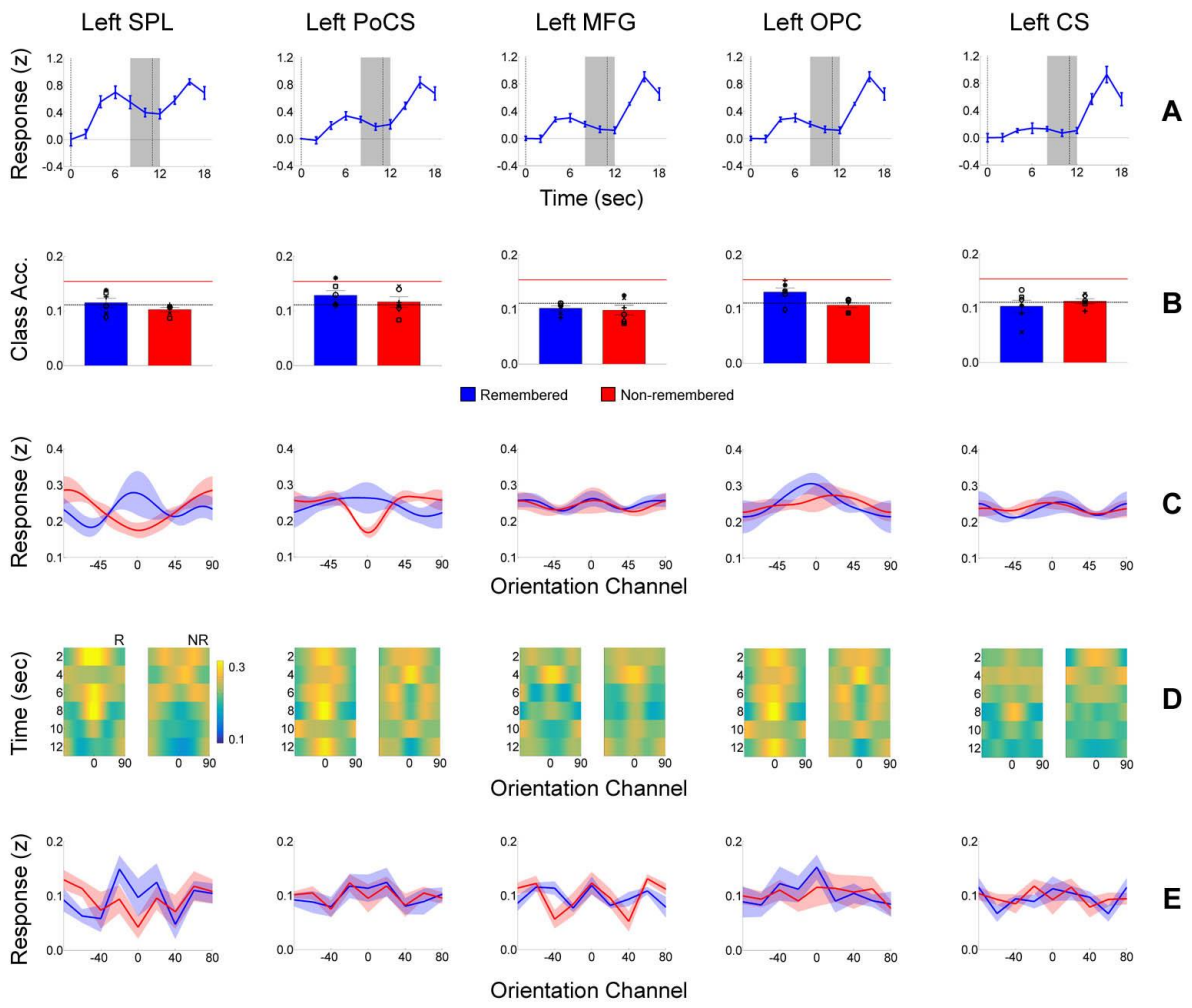

Figure S3 (Part 2) Representations of the remembered and non-remembered orientations in cortical regions with elevated delay period activation. Related to Figure 4. We used a random-effects general linear model containing regressors marking the sample, delay, and probe epochs to identify cortical regions showing elevated delay period activation (see Supplemental Experimental Procedures). Row A: estimated BOLD responses time-locked to the onset of the sample display. The vertical dashed lines at 0 and 11 seconds mark the onsets of the sample and probe displays, respectively. The shaded grey region marks data points used for subsequent multivariate analyses in rows C-F. Error bars are ±1 within-participant S.E.M. Row B: multivariate classification accuracy for the remembered and non-remembered orientations. Black symbols correspond to individual participants. The horizontal dashed line at 0.1111 marks idealized chance-level classification accuracy, while the horizontal red line at approximately 0.15 marks empirical chance-level classifier performance given the number of trials that each participant performed (see Supplemental Experimental Procedures). Row C: reconstructions of

the remembered and non-remembered orientations obtained using an inverted encoding model. Shaded areas are ±1 within-participant S.E.M. Row D: Reconstructions of the remembered ("R") and non-remembered ("NR") orientation on a sample-by-sample basis. All panels are on the same color scale (see color bar). Row E: reconstructions of the remembered and non-remembered orientations obtained using a basis set of Kroeneker delta functions. Shaded areas are ±1 within-participant S.E.M.

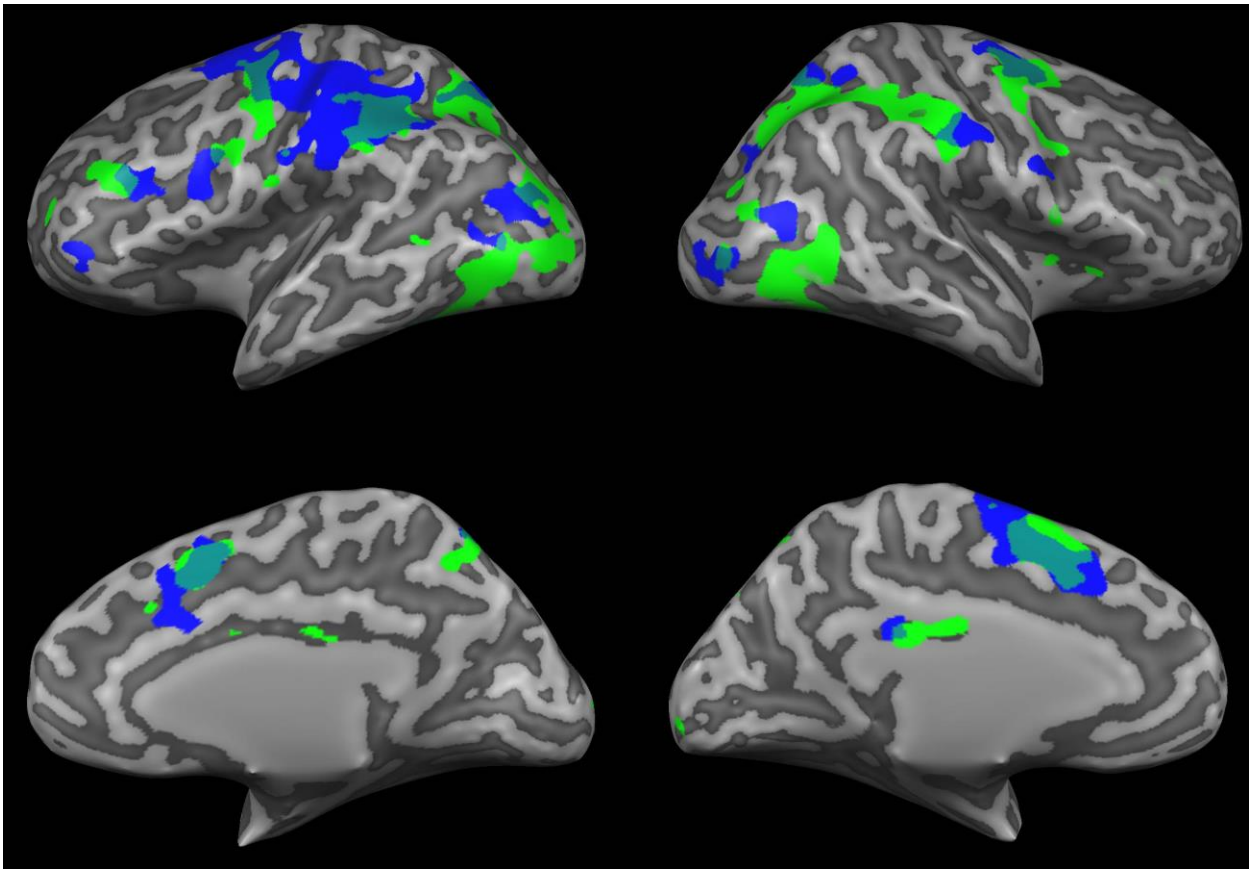

Figure S4. Cortical ROIs with robust sample-period (green) and delay-period (blue) activation. Related to *Identifying delay period-responsive ROIs*, Supplemental Experimental Procedures. Maps were thresholded at t(5) = 2.57, $p = 0.05$, uncorrected.

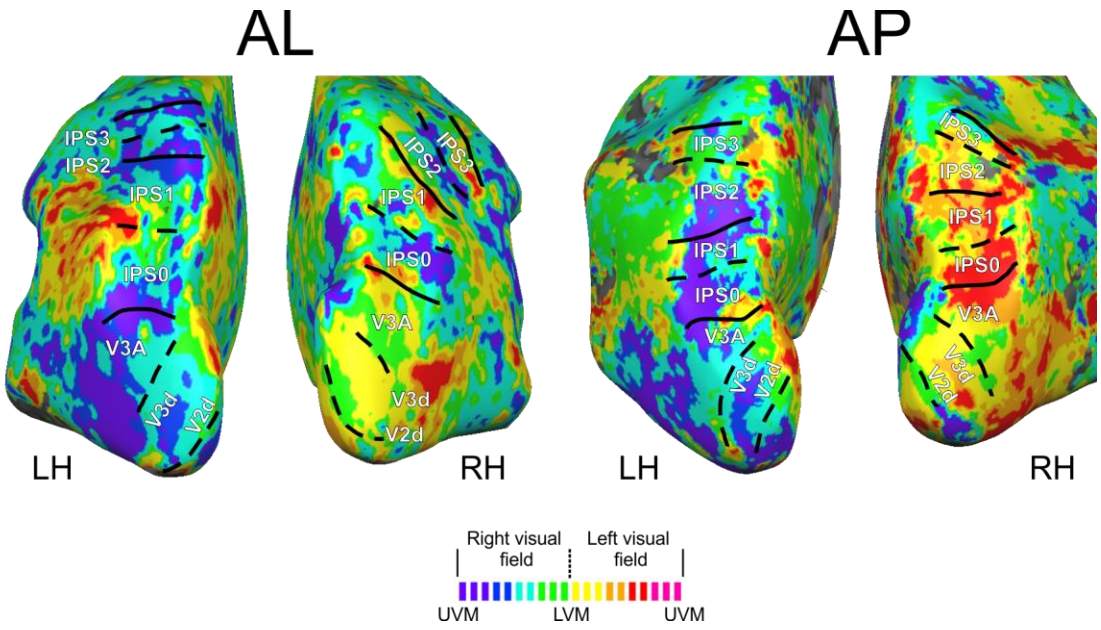

Figure S5. Retinotopic maps of IPS subregions for participants AL and AP. Related to *Retinotopic Mapping*, Supplemental Experimental Procedures. Maps for participants AA, AB, AC, and AI can be found in Figure S7 of Sprague and Serences (2013).

ROI	Contra R	Contra NR	Contra R > NR	Ipsi R	Ipsi NR	Ipsi R > NR
V1	5e-04	0.663	0.002	0.009	0.165	0.191
V2	0.171	0.696	0.105	0.069	0.262	0.278
V3	0.200	0.710	0.132	0.140	0.384	0.281
hV4v	0.034	0.816	0.007	0.453	0.258	0.613
V3a	0.164	0.164	0.524	0.132	0.463	0.246
IPS0	0.183	0.494	0.320	0.056	0.257	0.303
IPS1	0.325	0.229	0.525	0.076	0.492	0.139
IPS2	0.136	0.101	0.596	7e-04	0.418	0.064
IPS3	0.261	0.017	0.786	0.001	0.134	0.201

Table S1. Statistical comparisons of reconstructed representations of the remembered and non-remembered orientations in subregions of visual and posterior parietal cortex. Related to *Reconstructions of Orientation in Retinotopically Organized Visual and Posterior Parietal Cortex,* Results. R and NR show p-values depicting the robustness of the remembered and non-remembered orientations, respectively (see *Quantification and comparison of reconstructed representations* in Experimental Procedures). For R, a p-value < 0.05 corresponds to a robust (greater than zero) representation. For NR, a p-values < 0.05 indicates that the amplitude of the non-remembered orientation reconstruction was reliably less than 0. R>NR shows p-values comparing the strengths of remembered and non-remembered reconstructions. A p-value < 0.05 means that the reconstruction of the remembered orientation was significantly larger than the reconstruction of the non-remembered orientation.

Delay Period ROIs				Searchlight ROIs			
ROI	**R**	**NR**	**R>NR**	**ROI**	**R**	**NR**	**R>NR**
LH Ventromedial Cingulate	0.524	0.130	0.791	LH dlPFC	0.344	0.004	0.135
LH Superior Parietal Lobule	0.267	0.825	0.121	LH vlPFC	0.001	0.318	0.025
LH Lateral PFC	0.513	0.212	0.737	RH dlPFC	0.002	0.644	0.066
LH Postcentral Sulcus	0.099	0.662	0.102				
LH Central Sulcus	0.172	0.084	0.607				
LH Superior Precentral Sulcus	0.001	0.937	8e-04				
LH Medial Superior FG	0.292	0.690	0.270				
LH Occipitoparietal Cortex	0.050	0.299	0.146				
RH Postcentral Sulcus	0.319	0.994	0.027				
RH Occipitoparietal Sulcus	0.082	0.773	0.060				
RH Superior Precentral Sulcus	0.215	0.557	0.347				
RH Intraparietal Sulcus	0.114	0.317	0.309				
RH Medial Superior FG	0.300	0.435	0.406				
RH Superior Parietal Lobule	0.094	0.880	0.029				

Table S2. Statistical comparisons between representations of the remembered and non-remembered orientations omitting data from the third session. Related to *Quantification and comparison of reconstructed representations*, Experimental Procedures. R and NR show p-values depicting the robustness of the remembered and non-remembered orientations, respectively (see *Quantification and comparison of reconstructed representations* in Experimental Procedures). For R, a p-value < 0.05 corresponds to a robust (greater than zero) representation. For NR, a p-values < 0.05 indicates that the amplitude of the non-remembered orientation reconstruction was reliably less than 0. R>NR shows p-values comparing the strengths of remembered and non-remembered reconstructions. A p-value < 0.05 means that reconstructions of the remembered orientation was significantly stronger than reconstructions of the non-remembered orientation. PFC, prefrontal cortex. FG, frontal gyrus. dlPFC, dorsolateral prefrontal cortex. vlPFC, ventrolateral prefrontal cortex. LH, left hemisphere. RH, right hemisphere.

Supplemental Experimental Procedures

fMRI Acquisition & Preprocessing. Imaging data were acquired with a 3.0T GE MR 750 scanner located at the Center for Functional Magnetic Resonance Imaging on the UCSD campus and a 32 channel Nova Medical (Wilmington, MA) head coil. During WM scans we acquired whole-brain echo-planar images (EPIs) with a voxel size of 3 x 3 x 3 mm (192 x 192 mm field of view, 64 x 64 matrix size, 90° flip angle, 2000 ms TR, 30 ms TE, 35 3 mm-thick oblique slices with no gap). These data were subsequently resampled to a resolution of 2 x 2 x 2 mm. During retinotopic mapping scans (see below) we acquired EPIs with a resolution of 2 x 2 x 3 mm (192 x 192 mm field of view, 96 x 96 matrix size, 90° flip angle, 2250 ms TR, 30 ms TE, 31 3 mm-thick oblique slices with no gap) positioned over visual and posterior parietal cortex. All functional scans were coregistered to a separate anatomical scan (FSPGR T1-weighted sequence, 11 ms TR, 3.3 ms TE, 1100 ms TI, 172 slices, 18° flip angle, $1mm^3$ resolution) collected during a different session by first aligning each session's functional image to the anatomical scan collected in the same session, then aligning this anatomical scan to a target anatomical scan. EPI images were unwarped using FSL (Oxford, UK), slice-time corrected, motion corrected, high-pass filtered (to remove first, second, and third-order drift), transformed to Talairach space, and normalized (z-score) on a block by block basis.

Identifying delay period-responsive ROIs. We identified regions with elevated delay period activity (relative to resting baseline) using a random-effects general linear model (GLM). We first generated a model containing three boxcar regressors marking the sample, delay, and probe epochs of each trial. Each regressor was convolved with a canonical hemodynamic response function (the double-gamma function supplied by BrainVoyager; time-to-peak 5s, undershoot ratio 6:1, time-to-undershoot peak 16s) to generate a predicted response function. β coefficients for each regressor were then estimated using ordinary least squares (as implemented by BrainVoyager's built-in "Multi Study, Multi Subject" analysis package). The estimated β coefficients on each regressor were then entered into a one-tailed, repeated-measures t-test against a distribution with a mean of 0 (to maximize sensitivity, we did not correct the outcome of this analysis for multiple comparisons). We then generated a statistical parametric map (SPM) of t-scores for the sample and delay period β regressors and projected these data onto a computationally inflated representation of one participant's cortical surface (AI). As shown in

Figure S4, we observed robust sample- and delay period activity in a broad network of visual, superior parietal, and lateral frontal cortical regions.

ROIs with elevated delay period activation were formally defined using BrainVoyager's "Create POIs from Map Clusters" function with an area threshold of 20 mm^2. Where appropriate, large continuous ROIs (e.g., the large ROI spanning left central, precentral, and postcentral sulcus, as well as portions of medial superior frontal gyrus) cluster of three ROIs located near the intersection of right lateral parietal and right superior temporal cortex; Figure 3). Likewise, small neighboring clusters (e.g., the small ROIs located near the border of occipital and parietal cortex in both hemispheres; Figure 3) were combined into a single ROI. From this analysis, we identified a set of 14 unique ROIs with elevated delay period activation (see Figure 3 and Table 1). Note that because of variability in the shape of each participants grey-white matter boundary, the 3D coordinates of each ROI vary somewhat across participants. The mean (±1 S.E.M.) Talariach coordinates and sizes (i.e., number of voxels) for each ROI are listed in Table 1.

Retinotopic Mapping. Retinotopically organized visual areas V1-hV4v/V3a and posterior parietal areas IPS0-3 were defined using standard procedures (Engel et al., 1994; Sereno et al., 1995; Jerde et al., 2012; Sprague & Serences, 2013). Retinotopically organized posterior regions of the intraparietal sulcus (IPS; regions 0-3) using an attention-demanding mapping task. Participants were shown a rotating wedge stimulus (period = 24.75 s or 36 s) subtending 72˚ polar angle with an eccentricity spanning 1.75 to 8.75˚ from fixation. In alternating blocks the wedge contained a 4 Hz phase-reversing checkerboard stimulus or a field of moving dots; five participants completed between 10 (i.e., 5 checkerboard, 5 moving dots) and 14 blocks of these tasks. The remaining participant completed a total of 6 checkerboard blocks. EPIs were preprocessed as described above. To compute the best polar angle for each voxel in IPS we computed the power and phase at the stimulus frequency (1/24.75 Hz or 1/36 Hz) and subtracted the estimated hemodynamic response function delay (6.75 s) to align the signal phase in each voxel with the stimulus' position. Data from the dorsal and ventral portions of V2 and V3 were combined into single ROIs (i.e., V2, V3). Retinotopic maps showing the borders of IPS0-3 for participants AL

and AP are presented in Figure S5. Maps for the remaining participants can be found in Supplementary Figure 7 of Sprague and Serences (2013).

Multivariate Classification. All classification analyses were performed using libSVM software (Chang & Lin, 2011), available at http://www.csie.ntu.edu.tw/~cjlin/libsvm. Support vector machines (SVMs) were constructed using a radial basis function kernel, which captures both linear and non-linear relationships between condition labels and activation patterns. However, equivalent results were obtained when we used a linear kernel. We used the default cost and gamma parameter values supplied by the software (1 and 1/number_of_features, respectively). Qualitatively similar results were obtained when we used a cross-validation routine to find optimal values for these parameters. We performed leave-one-run-out cross-validation to ensure data used to train the classifier (all runs but one) and data classified (the held-out run) were statistically independent. All classification analyses were performed on each session separately, and classification accuracies were averaged across sessions. The significance of classifier performance was evaluated using a binomial distribution. We chose this approach because evaluating classifier performance using standard inferential statistics (e.g., t-tests against theoretical chance level decoding accuracy) can be misleading with a small number of observations (see Combrisson & Jerbi, 2015, for a detailed discussion of this issue). Given a probability *p* of obtaining a correct classification by chance (where *p* is one divided by the number of possible outcomes), the probability of observing *k* correct classifications by chance in *n* trials is given by:

$$P(k) = \frac{n!}{(n-k)!k!} p^k (1-p)^{n-k} \qquad \text{(Equation 1)}$$

Curve Fitting. Reconstructed representations were quantified by fitting them with the exponentiated cosine function described by Equation 4 in the main text). Fitting was performed by combining a general linear model with a grid search procedure. We first defined a range of plausible *k* values (from 3-40 in 0.1 increments). For each possible value of *k*, we generated a response function using Equation 5 after setting α and β to 1 and 0, respectively. Because trial-by-trial reconstructions of the remembered and non-remembered orientations were shifted to a

common center at 0°, we fixed μ at this value. Next, we generated a design matrix containing this response function and a constant term (i.e., a vector of ones) and used ordinary least squares regression to obtain estimates of α and β (defined as the regression coefficients for the response function and constant terms, respectively). The best fitting parameters were defined as those that minimized the sum of squared errors between the response function and the actual data.

References

Chung, C-C., & Lin, C-J. (2011). LIBSVM: a library for support vector machines. ACM Transactions on Intelligent Systems and Technology, *2* (3), 1-27.

Engel, S.A., Rumelhart, D.E., Wandell, B.A., Lee, A.T., Glover, G.H., Chichilnisky, E-J.,and Shadlen, M.N. (1994). fMRI of human visual cortex. Nature *369*, 525-527.

Combrisson, E., & Jerbi, K. (2015). Exceeding chance level by chance: The caveat of theoretical chance levels in brain signal classification and statistical assessment of decoding accuracy. J Neurosci Methods, doi: 10.1016/j.jneurmeth.2015.01.010.

Sereno, M.I., Dale, A.M., Reppas, J.B., Kwong, K.K., Belliveaw, J.W., Brady, T.J., Rosen, B.R., and Tootell, RB. (1995). Borders of multiple visual areas in humans revealed by functional magnetic resonance imaging. Science *268*, 889-893.